We also evaluated the mean concentration required for 50% growth inhibition (GI_{50}), which is defined as in (*34*, *35*), in a human cell panel composed of 37 cancer cell lines (fig. S5), and investigated the correlation between GI_{50} and expression of 26 genes that we selected on the basis of their potential association with the pharmacological activity of platinum compounds (*36*). The cytotoxic activity of oxaliplatin was inversely correlated with the expression of metallothionein (MT1Q) and methionine synthase (MTR), which are found in the cytoplasm and inactivate platinum compounds. DACHPt/m cytotoxicity did not exhibit similar correlations (table S1). We conclude that DACHPt/m may bypass cytoplasmic detoxification by MTR and MT1Q and efficiently deliver active platinum complexes to the nucleus, because they are internalized by endocytosis and selectively release the active platinum complexes in the late endosome/lysosome compartment (Fig. 1B).

Effect of DACHPt/m on oxaliplatin resistance in vitro

Our proposed mechanism of action of DACHPt/m led us to investigate their efficacy in oxaliplatin-resistant cancer cells, because MTR and MT1Q are overexpressed in these cells (*37*–*39*). We developed oxaliplatin-resistant HT29 cells (HT29/ox) by chronic exposure of HT29 cells to oxaliplatin with gradual dose escalation. Relative to the parental HT29 cells, HT29/ox cells were 10 times as resistant to oxaliplatin (Table 1). Quantitative real-time reverse transcription polymerase chain reaction (RT-PCR) and Western blotting revealed that the HT29/ox cells showed up-regulated messenger RNA (mRNA) as well as protein for MTR and MT1Q compared with HT29 cells (Fig. 4, A and B). Moreover, the down-regulation of MT1Q and MTR with small interfering RNA (siRNA) restored the sensitivity of HT29/ox cells to oxaliplatin (fig. S6). In vitro cytotoxicity studies showed that DACHPt/m was 120 times as cytotoxic as oxaliplatin in HT29/ox cells (Table 1). These results suggested that DACHPt/m may overcome acquired resistance to oxaliplatin.

In vivo intratumoral imaging of F-DACHPt/m in a human colon cancer model

DACHPt/m would need to extravasate, penetrate into the interstitial tissue, and be internalized by cancer cells after systemic administration to exert the in vivo antitumor activity predicted from the results above. We performed real-time intravital observation of the accumulation and subcellular fate of F-DACHPt/m in HT29 xenografts by using in vivo CLSM equipped with a high-speed resonant scanner developed to acquire live tissue images of experimental animals (fig. S7). Immediately after intravenous injection, F-DACHPt/m was observed in the blood vessels of solid tumors (Fig. 5A and video S2). The fluorescence from F-DACHPt/m in the blood vessels corresponded only to that of BODIPY FL. Even 12 hours later, only BODIPY FL fluorescence was observed flowing in the blood vessels (Fig. 5B and video S3). These observations indicate that F-DACHPt/m stably circulates in the bloodstream while maintaining their micellar structure. Images of tumor tissue revealed the accumulation and dissociation behaviors of F-DACHPt/m (Fig. 5, C and D, and video S3). Two hours after injection, F-DACHPt/m accumulated within the tumor tissue because of the EPR effect and was identified within the cells, whereas BODIPY TR fluorescence remained quenched. BODIPY TR fluorescence gradually appeared inside the cells 4 hours after injection and was clearly visible after 12 hours, indicating the release of DACHPt

Table 1. In vitro cytotoxicity of free oxaliplatin and DACHPt/m against HT29 and HT29/ox cells after a 48-hour incubation. Data are expressed as means ± SEM (n = 4).

Cells	IC_{50} (μM)*		
	Free oxaliplatin	DACHPt/m	Oxaliplatin/DACHPt/m
HT29	2.2 ± 2.2	0.47 ± 0.05	4.7
HT29/ox	22.8 ± 2.6	0.19 ± 0.11	120
Ratio of HT29/ox/HT29	10.4	0.4	—

*IC_{50} values obtained from the MTT assay.

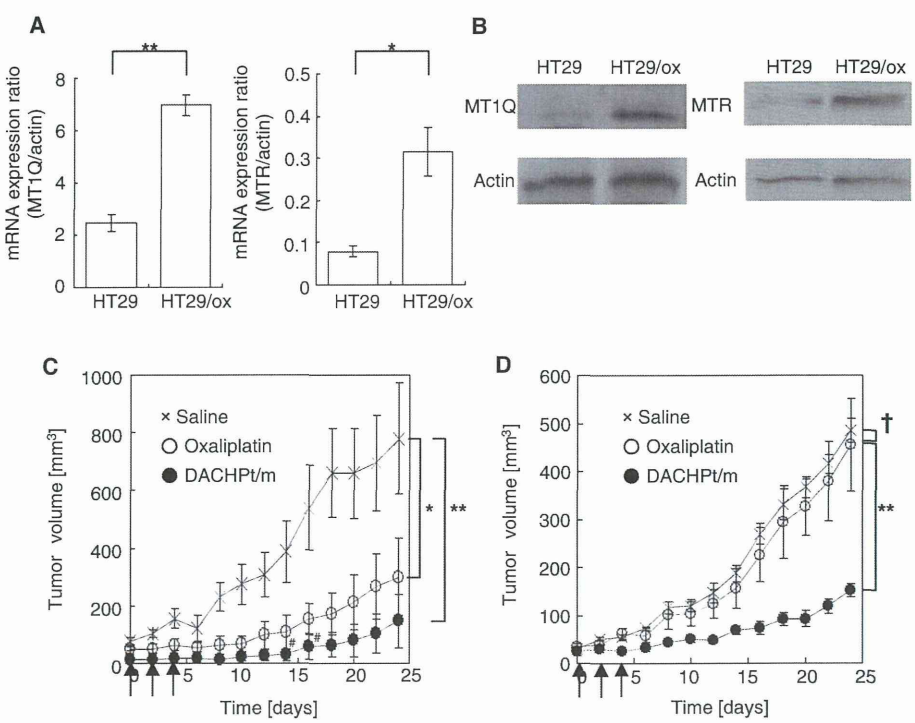

Fig. 4. Expression of MT1Q and MTR in HT29/ox cells and effects of DACHPt/m on HT29 and HT29/ox tumors in vivo. (**A**) Relative mRNA expression of metallothionein (MT1Q) and methionine synthase (MTR) in parent HT29 and HT29/ox cell lines. Data are expressed as means ± SEM (n = 3). *P < 0.05; **P < 0.01. (**B**) Western blots of MT1Q and MTR in HT29 and HT29/ox cell lines. (**C** and **D**) In vivo effect of DACHPt/m on subcutaneous HT29 (C) and HT29/ox (D) tumor cells. Crosses, saline; open circles, oxaliplatin (8 mg/kg); filled circles, DACHPt/m (4 mg/kg); arrows, injection of oxaliplatin and DACHPt/m; #, tumor regression; †P > 0.1; *P < 0.05; **P < 0.01. Data are expressed as means ± SEM (n = 4).

from the micelles inside the cells in the tumor tissue. The cell membrane, stained with CellMask, and cell nuclei were substantially free of F-DACHPt/m (Fig. 5, C and D, and video S3). These results were consistent with our in vitro results (Fig. 3A) and suggested that F-DACHPt/m percolated into interstitial tissues and was efficiently internalized to endosomal compartments of cells in a micelle form, followed by dissociation of the multimolecular structure of the micelles in the late endosomal and lysosomal compartments.

DACHPt/m enhances antitumor activity and overcomes oxaliplatin resistance in vivo

On the basis of our observations of the in vivo behavior of F-DACHPt/m, we hypothesized that DACHPt/m may also overcome oxaliplatin resistance in vivo. Thus, we evaluated DACHPt/m in vivo antitumor activity against subcutaneous HT29 and HT29/ox tumors (Fig. 4, C and D). Although free oxaliplatin failed to inhibit the growth of HT29/ox tumors, DACHPt/m exhibited substantial antitumor activity in the oxaliplatin-resistant xenograft model and successfully overcame the oxaliplatin resistance of HT29/ox cells in vivo (Fig. 4D). Note that DACHPt/m also achieved higher antitumor activity than oxaliplatin against the HT29 tumors (Fig. 4C). Thus, our micelle-based drug delivery vehicle was able to circumvent the detoxification mechanisms against platinum drugs in tumor cell cytoplasm through selective subcellular drug release and hence overcome acquired resistance.

DISCUSSION

Colorectal cancer is a major cause of morbidity and mortality worldwide (*1*). Oxaliplatin is currently the standard therapy for colorectal cancer, and acquired resistance to oxaliplatin is a major clinical drawback in the treatment of colorectal cancer [virtually all metastatic colorectal cancer becomes resistant to oxaliplatin, with a median time to progression of 8.7 months (*40*)]. The major cellular processes by which oxaliplatin enters and attacks cancer cells include uptake and transport, formation of DNA adducts and their recognition by damage response proteins, and signal transduction leading to apoptosis. Any factors that interfere with these pathways can lead to drug resistance (*41*). Here, we showed that DACHPt/m can overcome drug resistance by circumventing recognition by MTR and MT1Q, and achieve subcellular drug delivery both in vitro and in vivo to the perinuclear region of cells. It has been reported that drug delivery systems can overcome multidrug resistance

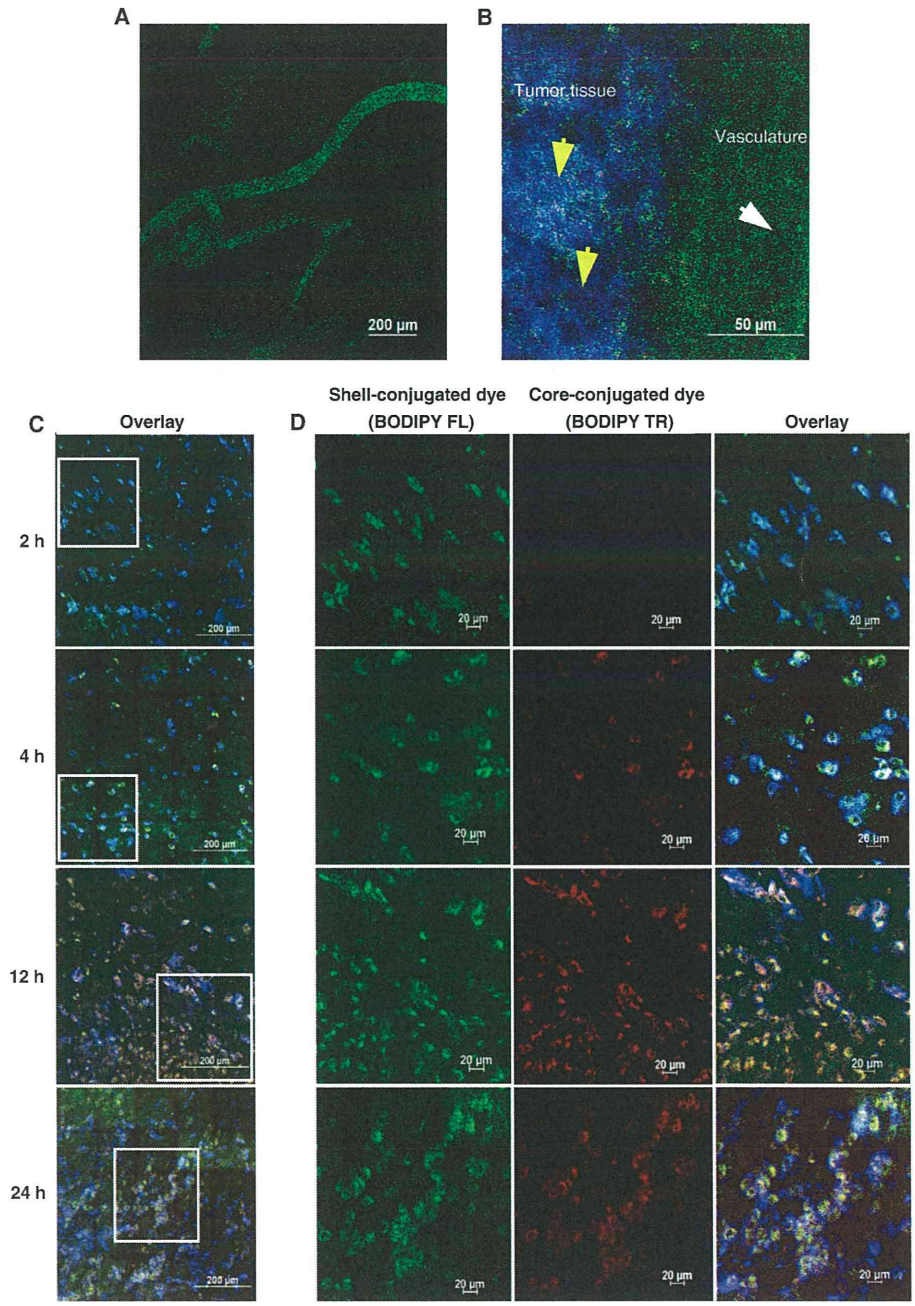

Fig. 5. In vivo CLSM observation of F-DACHPt/m in blood vessels and tumors after intravenous administration. (**A** and **B**) CLSM observation of F-DACHPt/m in the blood vessels of solid tumors (A) immediately after injection and (B) in the tumor tissue at 12 hours after injection. Yellow arrows, tumor tissue; white arrow, blood vessel. (**C**) Time-dependent CLSM observation of F-DACHPt/m in the tumor tissues at 2, 4, 12, and 24 hours after injection. Green, fluorescence from the shell-conjugated dyes (BODIPY FL); red, core-conjugated dyes (BODIPY TR); blue, cell surfaces stained by CellMask. (**D**) Magnification of selected areas [square regions in (C)] by channel.

by avoiding the drug efflux mechanism of P-glycoprotein (*20–22*). Because P-glycoprotein is not associated with platinum drug resistance (*42*), we used a different approach. Our data indicate that cytoplasmic detoxification mechanisms against platinum drugs can potentially be avoided by using the appropriate drug delivery system.

Nanocarriers encounter numerous barriers in vivo en route to their target during the processes of blood circulation, extravasation, penetration, and cellular uptake. It is therefore difficult to extrapolate in vivo outcomes of a drug-nanocarrier combination from its in vitro behavior, although real-time observation of in vivo behaviors such as we have used here can ascertain critical barriers residing in a living body and facilitate the design of a nanocarrier optimized for in vivo delivery. The in vivo CLSM technique that we used in this study enabled spatiotemporal and quantitative analyses of extravasation, tissue penetration, and cellular internalization of nanocarriers in living animals. Using dual fluorescent labeling of DACHPt/m, we elucidated the real-time intratumoral behavior of DACHPt/m. The dual fluorescent label of DACHPt micelles allowed us to trace the micelles' position by the ever-present fluorescent signal from the surface of the micelles, and the drug release and dissociation of the multimolecular structure of the micelles by the dequenching and fluorescence recovery of the core-conjugated dye. In in vitro cellular experiments, these micelles were internalized intact, and then they were disassembled and the drug was released in late endosomes. In our in vivo microscopy, we observed that DACHPt/m maintained their micelle form during circulation in the blood, probably because of the stable inner core structure formed by the polymer-metal complexes, and extravasated into solid tumors. DACHPt/m was able to deeply penetrate cancerous tissue after extravasation and was internalized by different cell populations that were distant from the blood vessels. Such efficient penetration of tissue is a requirement of successful drug delivery and a prerequisite for effective subcellular targeting. It has been reported that PEG-modified liposomes with 100-nm diameter accumulated at perivascular regions of solid tumors and failed to penetrate the tumor interstitium deeply (*43*). Although this characteristic may depend on the cancer type, it is possible that the deep tumor penetration of DACHPt/m is a result of their smaller 30-nm size. Finally, the DACHPt/m structure dissociated at the perinuclear regions of the cell after internalization, based on the pH and chloride ion concentration–selective release of DACHPt. This observation is also consistent with our hypothesis that DACHPt/m can overcome oxaliplatin resistance in tumors by bypassing the cytoplasmic detoxification mechanisms of MTR and MT1Q. There are, however, several limitations to the type of study that we have performed in a subcutaneous tumor model. Compared with subcutaneous tumors, orthotopic and spontaneously forming tumors may have characteristic differences such as vascular density and degree of fibrosis, which may affect the transport of nanocarriers (*44*).

Our research provides one approach for subcellular targeting of cytoplasmic drugs. Such nanocarriers have the potential to enhance the drug efficacy and overcome drug resistance.

MATERIALS AND METHODS

Materials

γ-Benzyl L-glutamate and bis(trichloromethyl) carbonate (triphosgene) were purchased from Sigma Chemical and Tokyo Kasei Kogyo, respectively. *N,N*-Dimethylformamide (DMF), 3-(4,5-dimethylthiazol-2-yl)-2,5-diphenyltetrazolium bromide (MTT), and dimethyl sulfoxide (DMSO) were purchased from Wako Pure Chemicals. Oxaliplatin and $NaCH_3CN$ were purchased from Sigma-Aldrich Inc. Dichloro(1,2-diammino cyclohexane) platinum(II) was purchased from W. C. Heraeus GmbH. α-Methoxy-ω-amino-poly(ethylene glycol) [CH_3O-PEG-NH_2; molecular weight (MW), 12,000] was purchased from Nippon Oil and Fats. BODIPY TR-succinimidyl ester, BODIPY FL-hydrazide, LysoTracker Blue, CellLight Early Endosome-RFP (Rab5a-RFP), CellMask, and Lipofectamine RNAiMAX were purchased from Invitrogen.

Cell lines and animals

HT29 cells were purchased from the American Type Culture Collection. HT29 cells were maintained in McCoy's 5A modified medium (Invitrogen) containing 10% fetal bovine serum (Gibco) as well as 1% penicillin and streptomycin (Sigma) and were cultured at 37°C in a humidified atmosphere of 5% CO_2. To develop HT29/ox cells (*45*), we treated HT29 cells with oxaliplatin at IC_{50} doses for 1 hour. After 24 hours, cells were subcultured into new flasks and oxaliplatin was added to a culture of 80% confluent cells. The concentration was incrementally increased by factors of 1.2 to 2. The process was continued until the cells were resistant to drug concentrations at least 10 times as great. BALB/c-nu/nu mice (female; body weight, 18 to 20 g; age, 6 weeks old) were purchased from Charles River Japan. All animal experiments were carried out in accordance with the guidelines for animal experiments at the University of Tokyo, Japan.

Methods

Synthesis of block copolymers. α-4-(Diethoxymethyl)benzyl-ω-amino-poly(ethylene glycol) (Ac-Bz-PEG-NH_2) was previously synthesized in our laboratory (*46*). Poly(ethylene glycol)-*b*-poly(L-glutamic acid) [PEG-*b*-P(Glu)] [MW_{PEG}, 12,000; polymerization degree of P(Glu), 20] and Ac-Bz-PEG-*b*-poly(L-glutamic acid) [Ac-Bz-PEG-*b*-P(Glu)] [MW_{PEG}, 12,000; polymerization degree of P(Glu), 20] were synthesized according to the previously described synthetic method (*47*). Briefly, *N*-carboxyanhydride of γ-benzyl L-glutamate (BLG-NCA) was synthesized by the Fuchs-Farthing method with triphosgene (*48*). BLG-NCA was polymerized in DMF initiated by the amino group of CH_3O-PEG-NH_2 or Ac-Bz-PEG-NH_2 to obtain PEG-*b*-poly(γ-benzyl L-glutamate) (PEG-*b*-PBLG) or Ac-Bz-PEG-*b*-PBLG, respectively. The MW distribution of PEG-*b*-PBLG and Ac-Bz-PEG-*b*-PBLG was determined by gel permeation chromatography (GPC) [column, TSK-gel G3000HHR, G4000HHR (Tosoh); eluent, DMF containing 10 mM LiCl; flow rate, 0.8 ml/min; detector, refractive index; temperature, 25°C]. PEG-*b*-PBLG and Ac-Bz-PEG-*b*-PBLG showed narrow MW distributions (M_w/M_n: 1.09 and 1.16, respectively) in GPC. The degrees of polymerization of PBLG in PEG-*b*-PBLG and Ac-Bz-PEG-*b*-PBLG were determined to be 20 by comparing the proton ratios of methylene units in PEG (-OCH_2CH_2-: δ = 3.7 ppm) and phenyl groups of PBLG (-$CH_2C_6H_5$: δ = 7.3 ppm) in ^{1}H-NMR (nuclear magnetic resonance) measurement. Both PEG-*b*-PBLG and Ac-Bz-PEG-*b*-PBLG were deprotected by mixing with 0.5 N NaOH at room temperature to obtain PEG-*b*-P(Glu) and Ac-Bz-PEG-*b*-P(Glu), respectively. Complete deprotection was confirmed by ^{1}H NMR measurement.

Preparation of micelles. For conjugation of BODIPY TR to a polymer, a solution of BODIPY TR-succinimidyl ester in DMSO (1 mg/ml) was mixed with Ac-Bz-PEG-*b*-P(Glu). The reaction was carried out overnight at room temperature with stirring. Unreacted

BODIPY TR was removed by dialysis [MW cutoff (MWCO) size, 2000 daltons] against DMSO and water. To conjugate BODIPY FL to the Ac-Bz-PEG-*b*-P(Glu)-BODIPY TR polymer, we mixed a solution of BODIPY FL-hydrazide in DMSO with the polymer, followed by the addition of 1 N HCl to deprotect the acetal group. Samples were stirred overnight at room temperature and treated with $NaBH_3CN$ to reduce the link between BODIPY FL and the polymer. For purification, unbound BODIPY FL was removed by dialysis (MWCO, 2000 daltons) against DMSO and water. The prepared BODIPY FL-PEG-*b*-P(Glu)-BODIPY TR copolymer was freeze-dried overnight and stored at −20°C. DACHPt/m and F-DACHPt/m were prepared according to the previously described method (*23*). DACHPt (5 mM) was suspended in distilled water and mixed with silver nitrate ([$AgNO_3$]/[DACHPt] = 1) to form aqueous complexes. The solution was kept in the dark at 25°C for 24 hours. AgCl precipitates were eliminated by centrifugation. The supernatant was purified by passage through a 0.22-μm filter. DACHPt aqueous complex solution was then mixed with PEG-*b*-P(Glu) or BODIPY FL-PEG-*b*-P(Glu)-BODIPY TR ([Glu] = 5 mM; [DACHPt]/[Glu] = 1.0) and reacted for 120 hours to obtain DACHPt/m or F-DACHPt/m, respectively. DACHPt/m and F-DACHPt/m were purified by ultrafiltration (MWCO, 30,000 daltons; Fig. 1A). The size distributions of DACHPt/m and F-DACHPt/m were evaluated by dynamic light scattering at 25°C with a Zetasizer Nano ZS90 (Malvern Instruments). The platinum content of DACHPt/m was determined by ion-coupled plasma mass spectrometry (4500 ICP-MS; Hewlett Packard).

Drug release and fluorescence profiles of micelles under different conditions. The release of platinum from DACHPt/m and F-DACHPt/m in phosphate-buffered saline (PBS) at 37°C was evaluated as described (*23*). Briefly, a micelle solution of known platinum concentration was placed inside a dialysis bag (MWCO, 2000 daltons). The solution was then dialyzed against PBS under different conditions mimicking the extracellular environment (10 mM PBS, pH 7.4, and 150 mM NaCl), early endosomes (10 mM PBS, pH 6.9, and 20 mM NaCl), and late endosomes (10 mM PBS, pH 5.5, and 70 mM NaCl) at 37°C (*25*). The concentration of platinum present in the dialysate was determined with ICP-MS. The fluorescence profiles of F-DACHPt/m were also evaluated under the same conditions with a spectrofluorometer (FP6600, Jasco) or NanoDrop (ND3300, Scrum). Changes in fluorescence intensity were measured at a defined time period.

In vitro observation of subcellular localization and the fate of F-DACHPt/m by CLSM. HT29 cells were cultured at 1×10^5 cells in 35-mm glass-based dishes (Asahi Techno Glass). After overnight incubation in a fresh medium, the cells were washed twice with PBS. The medium was then replaced by 1 ml of fresh medium containing F-DACHPt/m (100 μM on Pt base). Live-cell CLSM imaging was performed with a Zeiss LSM 510 META nonlinear optics scan head attached to an inverted Axiovert 200 M SP equipped with a 63 × 1.4 numerical aperture Plan Apochromat oil immersion objective (Carl Zeiss). For long-term time-lapse imaging, culture dishes were wrapped with an optically clear foil cover (Carl Zeiss) to avoid evaporation and mounted onto the microscope stage incubator (37°C, 5% CO_2, 90% relative humidity). Bright-field DIC (differential interference contrast) images and fluorescent sequences were taken every 30 min for 72 hours. BODIPY FL was excited at 488 nm with an Ar laser and fluorescence was detected at 500 to 530 nm, whereas BODIPY TR was excited at 543 nm with a He-Ne laser, and fluorescence was detected at 565 to 615 nm. Laser power was kept low at 0.36 mW for 488 nm and at 0.018 mW for 543 nm so that photobleaching was negligible. To determine whether DACHPt/m was taken up by endocytosis, we treated HT29 cells with F-DACHPt/m at 37°C or 4°C for 6 hours and then observed by CLSM. For the colocalization studies, we used micelles prepared from BODIPY FL-PEG-P(Glu) that only emit fluorescence from the shell. HT29 cells, which had been preincubated with CellLight Early Endosome-RFP to express an early endosome marker, Rab5a-RFP, were treated with BODIPY FL–conjugated DACHPt/m, and images were taken at indicated time points after staining with LysoTracker Blue. Rab5a-RFP was excited at 543 nm with a He-Ne laser, and fluorescence was detected at 565 to 615 nm. LysoTracker Blue was excited in multiphoton mode at 710 nm with a Mai Tai tunable broadband laser (Spectra-Physics), and fluorescence was detected at 390 to 465 nm. Colocalization was quantified as follows:

$$\text{amount of colocalization (\%)} = \text{BODIPY FL pixels}_{\text{colocalization}}/\text{BODIPY FL pixels}_{\text{total}} \times 100$$

where BODIPY FL $\text{pixels}_{\text{colocalization}}$ represents the number of BODIPY FL pixels colocalizing with Rab5a-RFP or LysoTracker pixels in the cytoplasm, and BODIPY FL $\text{pixels}_{\text{total}}$ represents the number of all BODIPY FL pixels in the cytoplasm. The timing and location of the micelle dissociation and concomitant drug release were studied by evaluating the colocalization of BODIPY FL and BODIPY TR signals from F-DACHPt/m with the late endosomes/lysosomes (Fig. 3, E and F). Cells were treated with F-DACHPt/m, and images were taken at indicated time points after staining with LysoTracker Blue. Colocalization was quantified as follows:

$$\text{amount of colocalization (\%)} = \text{BODIPY FL or BODIPY TR pixels}_{\text{colocalization}}/\text{BODIPY FL or BODIPY TR pixels}_{\text{total}} \times 100$$

where BODIPY FL or BODIPY TR $\text{pixels}_{\text{colocalization}}$ represents the number of BODIPY FL or BODIPY TR pixels colocalizing with LysoTracker pixels in the cytoplasm, and BODIPY FL or BODIPY TR $\text{pixels}_{\text{total}}$ represents the number of all BODIPY FL or BODIPY TR pixels in the cytoplasm.

Determination of subcellular Pt accumulation and amount of Pt-DNA adducts. HT29 cells (6×10^6) were seeded in 100-mm tissue culture dishes. After 24 hours, cells were treated with 10 μM oxaliplatin or DACHPt/m on a platinum base. After 6, 8, 12, and 24 hours of drug exposure, the medium was removed and the cells were washed three times with PBS, scraped, and harvested. Samples were freeze-dried overnight, dissolved in heated nitric acid, and evaporated to dryness. The samples were redissolved in water and the Pt content was determined by ICP-MS. For the quantification of Pt-DNA adducts, DNA was extracted with a DNA purification kit (Promega) according to the manufacturer's protocol. The amount and purity of DNA were determined by measuring absorption at 260 and 280 nm with NanoDrop (ND3300). The DNA was dissolved in nitric acid, dried, and redissolved in water. The Pt content was determined by ICP-MS, and the DNA platination levels were expressed as micrograms of Pt per milligram of DNA.

In vitro cytotoxicity study against human cancer cells. The in vitro cytotoxicity of oxaliplatin and DACHPt/m was examined against a panel of 37 human cancer cells as described (*34*, *35*). Cancer cells were plated into flat-bottomed 96-well plates at 5×10^3 per well. Cells were treated by continuous exposure to oxaliplatin or DACHPt/m in a final volume of 100 μl. Plates were incubated for 48 hours at 37°C in a humidified atmosphere with 5% CO_2, and cell viability was determined

by MTT assay. To determine the relationship between cellular sensitivity to oxaliplatin or DACHPt/m and the expression of genes involved in the sensitivity or resistance of cells to platinum compounds, we assessed the gene expression profile of 21 human cancer cell lines for 26 genes selected on the basis of previous studies on cisplatin- or oxaliplatin-resistant cells (*36*). Expression of these individual genes was determined by searching the National Cancer Institute database. The coefficient of correlation between the GI_{50}s of free oxaliplatin and DACHPt/m as well as the level of gene expression was calculated for each gene.

Quantitative real-time RT-PCR. The expression of the metallothionein (MT1Q) [human MT1B (same as MT1Q), NM_005947, 4MQ-012725-01-0002] and methionine synthase (MTR) (human MTR, NM_000254, 4LQ-009896-00-0002) was confirmed by quantitative real-time RT-PCR. After 24 hours of treatment, cells were washed with PBS and harvested. Total RNA was prepared with TRIzol (Invitrogen), and complementary DNA (cDNA) was reverse-transcribed with a QuantiTect reverse transcription kit (Qiagen). PCR primer sequences were as follows: MT1Q, 5′-GAACTCCAGGCTTGTCTTGG-3′ (forward) and 5′-CATTTGCACTCTTTGCACTTG-3′ (reverse); MTR, 5′-ACCCAACTTCCAGGGAGACT-3′ (forward) and 5′-GGCAC-CATGATCTTGGACTT-3′ (reverse); actin, 5′-AGATGTGGATCAG-CAAGCAG-3′ (forward) and 5′-GCGCAAGTTAGGTTTTGTCA-3′ (reverse); and 18*S*, 5′-CGGCGACGACCCATTCGAAC-3′ (forward) and 5′-GAATCGAACCCTGATTCCCCGTC-3′ (reverse). cDNA from HT29 cells was amplified with specific primers with a SYBR Green Core Reagent Kit (Qiagen) and a real-time PCR instrument (Applied Biosystems). Expression of each gene was standardized with endogenous actin or 18*S* as a control, and its relative levels in HT29 or HT29/ox cells were quantified by calculating $2^{-\Delta\Delta C_T}$, where $\Delta\Delta C_T$ is the difference in C_T (cycle number at which the amount of amplified target reaches a fixed threshold) between target and reference.

MT1Q and MTR gene knockdown. The siRNAs against MT1Q and MTR and the control siRNA were purchased from Thermo Fisher Scientific Inc. The siRNA target sequences against MT1Q are the following: siMT1Q, GCAAAGGCUCAUCAGAGAA. The siRNA sequences against MTR are the following: siMTR, CUGAGAAGCU-CUUACGUUA. The siRNAs were transfected into the cell with Lipofectamine RNAiMAX (Invitrogen) according to the instructions of the manufacturer. Briefly, HT29/ox cells (4×10^5) were seeded in six-well plates. Twenty-four hours later, the mixture of siMT1Q (50 nM) and siMTR (50 nM) was transfected into the cells with Lipofectamine RNAiMAX reagent. Knockdown of MT1Q and MTR was separately confirmed by real-time PCR (fig. S6, A and B, respectively). To investigate the role of MT1Q and MTR in the oxaliplatin resistance in HT29/ox cells, we seeded HT29/ox cells (5×10^3) in 96-well plates, and 24 hours later, the mixture of siMT1Q (50 nM) and siMTR (50 nM) or the control siRNA was transfected into the cells with Lipofectamine RNAiMAX reagent. Twenty-four hours after transfection, the transfected HT29/ox cells were treated by continuous exposure to oxaliplatin in a final volume of 100 μl. Plates were further incubated for 48 hours at 37°C in a humidified atmosphere with 5% CO_2, and their cytotoxicity was determined by MTT assay.

Western blotting. HT29 or HT29/ox cells (5×10^6) were seeded in 100-mm^2 plates and washed with PBS (100 μl). Cell extracts were resolved in TNE buffer [1% NP-40, 150 mM NaCl, 10 mM tris-HCl, 1 mM EDTA, aprotinin (10 μg/ml), 2 mM Na_3VO_4, 10 mM NaF]. The cell suspension was centrifuged for 20 min at 15,000*g*. Sampling buffer (4×) was added to the aliquots, followed by incubation for 5 min at 100°C. Transfer to a polyvinylidene difluoride membrane (Invitrogen) was performed by electrophoresis for 90 min at 125 V. Membranes were blocked with 6% nonfat milk or tris-buffered saline (TBS) with 0.1% Tween 20 (MT1Q) for 1 hour. They were then probed at room temperature with the following antibodies: anti-metallothionein (ab12228, 1:1000, Abcam), anti–methionine synthase (ab66039, 1:2000, Abcam), and anti–β-actin (#4967, 1:1000, Cell Signaling). Membranes were washed three times with washing buffer (TBS with 0.1% Tween 20) and then probed with the secondary anti–rabbit immunoglobulin G (IgG) horseradish peroxidase (HRP) (W401B, 1:10,000, Promega) or anti–mouse IgG HRP (W402B, 1:10,000, Promega) conjugate for 1 hour. The secondary antibody was washed three times with washing buffer and then evenly coated with enhanced chemiluminescence (ECL) Western blotting detection reagents (GE Healthcare) for 30 s. The membrane was immediately exposed to Fuji Medical X-ray film (Fujifilm) at room temperature for various periods in a film cassette. Protein levels were standardized with the signal from the β-actin probe.

In vivo antitumor activity studies. BALB/c-nu/nu mice (female, $n = 4$) were inoculated subcutaneously with HT29 or HT29/ox cells (1×10^7/ml). Tumors were allowed to grow for 1 week (tumor size at this point was about 40 mm^3). Mice were then treated intravenously three times at 2-day intervals with oxaliplatin (8 mg/kg) or DACHPt/m (4 mg/kg) on a platinum base. Antitumor activity was evaluated in terms of tumor size (V) with the following equation:

$$V = a \times b^2/2$$

Here, a and b are the major and minor axes, respectively, of the tumor as measured by a caliper.

Intravital observation of the in vivo behavior of F-DACHPt/m. Intravital observation of F-DACHPt/m was performed as described (*49*). Female BALB/c mice (6 to 8 weeks old) were inoculated subcutaneously with HT29 cells (1×10^7/ml). After 5 days, when the tumor volumes reached 70 mm^3, F-DACHPt/m (10 mg/kg) was administered intravenously. At 2, 4, 12, and 24 hours after treatment, mice were anesthetized with 2.5% isoflurane (Abbott Japan) with a Univentor 400 Anesthesia Unit (Univentor). An arc-shaped incision was made around the subcutaneous tumor, and the skin flap was elevated without injuring the feeding vessels. The mouse was placed directly onto a thermoplate (Tokai Hit), and the skin flap was everted and stretched with several bent 30-gauge needles. The plasma membrane stain, CellMask Deep Red, was directly applied to the subcutaneous tumor, and a coverslip (Muto Pure Chemicals) was attached with just enough pressure to flatten the tumor surface. All in vivo images were acquired with a Nikon A1R CLSM attached to an upright Eclipse FN1 (Nikon). The A1R incorporates a conventional galvano scanner and a high-speed resonant scanner. The latter allows an acquisition speed of 30 frames per second while maintaining a relatively high resolution of 512 × 512 scanned points. BODIPY FL, BODIPY TR, and CellMask were excited with three lasers (488-nm Ar, 560-nm He-Ne, and 640-nm He-Ne lasers), and the fluorescent signals were detected. Laser powers were kept at 19.5 mW for 488-nm Ar, 7.5 mW for 561-nm He-Ne, and 1 mW for 640-nm He-Ne.

Statistical analysis. Data are presented as means ± SEM. The significant differences between the groups were analyzed by a Student's t test, and a P value of <0.05 was considered significant.

SUPPLEMENTARY MATERIAL

www.sciencetranslationalmedicine.org/cgi/content/full/3/64/64ra2/DC1

Fig. S1. Synthetic scheme of BODIPY FL-PEG-*b*-P(Glu)-BODIPY TR.

Fig. S2. Size distribution of DACHPt/m and F-DACHPt/m as determined by dynamic light scattering.

Fig. S3. Fluorescent images of HT29 cells after 6-hour incubation with F-DACHPt/m at 37°C and 4°C.

Fig. S4. In vitro CLSM observation of dissociation of F-DACHPt/m in the late endosomes/lysosomes.

Fig. S5. In vitro cytotoxicity of oxaliplatin and DACHPt/m against a human cancer cell panel.

Fig. S6. Knockdown of MT1Q and MTR restores the sensitivity of HT29/ox to oxaliplatin.

Fig. S7. Schematic illustration of experimental settings of in vivo CLSM.

Table S1. Coefficient of correlation between the GI_{50}s of free oxaliplatin or DACHPt/m and the expression levels of genes involved in the sensitivity or resistance of cells to platinum compounds.

Video S1. In vitro live imaging.

Video S2. In vivo live imaging (immediately after injection).

Video S3. In vivo live imaging (12 hours after injection).

REFERENCES AND NOTES

1. A. Jemal, R. Siegel, E. Ward, Y. Hao, J. Xu, M. J. Thun, Cancer statistics, 2009. *CA Cancer J. Clin.* **59**, 225–249 (2009).
2. T. M. Allen, P. R. Cullis, Drug delivery systems: Entering the mainstream. *Science* **303**, 1818–1822 (2004).
3. M. Ferrari, Cancer nanotechnology: Opportunities and challenges. *Nat. Rev. Cancer* **5**, 161–171 (2005).
4. V. P. Torchilin, Recent advances with liposomes as pharmaceutical carriers. *Nat. Rev. Drug Discov.* **4**, 145–160 (2005).
5. R. Duncan, The dawning era of polymer therapeutics. *Nat. Rev. Drug Discov.* **2**, 347–360 (2003).
6. Y. Matsumura, H. Maeda, A new concept for macromolecular therapeutics in cancer chemotherapy: Mechanism of tumoritropic accumulation of proteins and the antitumor agent Smancs. *Cancer Res.* **46**, 6387–6392 (1986).
7. M. E. Davis, Z. G. Chen, D. M. Shin, Nanoparticle therapeutics: An emerging treatment modality for cancer. *Nat. Rev. Drug Discov.* **7**, 771–782 (2008).
8. N. Nishiyama, K. Kataoka, Current state, achievements, and future prospects of polymeric micelles as nanocarriers for drug and gene delivery. *Pharmacol. Ther.* **112**, 630–648 (2006).
9. M. Yokoyama, M. Miyauchi, N. Yamada, T. Okano, Y. Sakurai, K. Kataoka, S. Inoue, Characterization and anticancer activity of the micelle-forming polymeric anticancer drug adriamycin-conjugated poly(ethylene glycol)-poly(aspartic acid) block copolymer. *Cancer Res.* **50**, 1693–1700 (1990).
10. K. Kataoka, G. S. Kwon, M. Yokoyama, T. Okano, Y. Sakurai, Block copolymer micelles as vehicles for drug delivery. *J. Control. Release* **24**, 119–132 (1993).
11. K. Kataoka, A. Harada, Y. Nagasaki, Block copolymer micelles for drug delivery: Design, characterization and biological significance. *Adv. Drug Deliv. Rev.* **47**, 113–131 (2001).
12. A. V. Kabanov, E. V. Batrakova, D. W. Miller, Pluronic block copolymers as modulators of drug efflux transporter activity in the blood–brain barrier. *Adv. Drug Deliv. Rev.* **55**, 151–164 (2003).
13. Y. Matsumura, K. Kataoka, Preclinical and clinical studies of anticancer agent-incorporating polymer micelles. *Cancer Sci.* **100**, 572–579 (2009).
14. Y. Matsumura, T. Hamaguchi, T. Ura, K. Muro, Y. Yamada, Y. Shimada, K. Shirao, T. Okusaka, H. Ueno, M. Ikeda, N. Watanabe, Phase I clinical trial and pharmacokinetic evaluation of NK911, a micelle-encapsulated doxorubicin. *Br. J. Cancer* **91**, 1775–1781 (2004).
15. T. Hamaguchi, K. Kato, H. Yasui, C. Morizane, M. Ikeda, H. Ueno, K. Muro, Y. Yamada, T. Okusaka, K. Shirao, Y. Shimada, H. Nakahama, Y. Matsumura, A phase I and pharmacokinetic study of NK105, a paclitaxel-incorporating micellar nanoparticle formulation. *Br. J. Cancer* **97**, 170–176 (2007).
16. T. Hamaguchi, T. Doi, T. Eguchi-Nakajima, K. Kato, Y. Yamada, Y. Shimada, N. Fuse, A. Ohtsu, S. Matsumoto, M. Takanashi, Y. Matsumura, Phase I study of NK012, a novel SN-38–incorporating micellar nanoparticle, in adult patients with solid tumors. *Clin. Cancer Res.* **16**, 5058–5066 (2010).
17. R. H. Wilson, R. Plummer, J. Adam, M. M. Eatock, A. V. Boddy, M. Griffin, R. Miller, Y. Matsumura, T. Shimizu, H. Calvert, Phase I and pharmacokinetic study of NC-6004, a new platinum entity of cisplatin-conjugated polymer forming micelles. *J. Clin. Oncol.* **26**, 2573 (2008).
18. R. Dent, M. Trudeau, K. I. Pritchard, W. M. Hanna, H. K. Kahn, C. A. Sawka, L. A. Lickley, E. Rawlinson, P. Sun, S. A. Narod, Triple-negative breast cancer: Clinical features and patterns of recurrence. *Clin. Cancer Res.* **13**, 4429–4434 (2007).
19. J. A. Hubbell, Materials science. Enhancing drug function. *Science* **300**, 595–596 (2003).
20. T. Minko, P. Kopecková, J. Kopecek, Efficacy of the chemotherapeutic action of HPMA copolymer-bound doxorubicin in a solid tumor model of ovarian carcinoma. *Int. J. Cancer* **86**, 108–117 (2000).
21. D. Kim, E. S. Lee, K. T. Oh, Z. G. Gao, Y. H. Bae, Doxorubicin-loaded polymeric micelle overcomes multidrug resistance of cancer by double-targeting folate receptor and early endosomal pH. *Small* **4**, 2043–2050 (2008).
22. K. Cho, X. Wang, S. Nie, Z. G. Chen, D. M. Shin, Therapeutic nanoparticles for drug delivery in cancer. *Clin. Cancer Res.* **14**, 1310–1316 (2008).
23. H. Cabral, N. Nishiyama, S. Okazaki, H. Koyama, K. Kataoka, Preparation and biological properties of dichloro(1,2-diaminocyclohexane)platinum(II) (DACHPt)-loaded polymeric micelles. *J. Control. Release* **101**, 223–232 (2005).
24. H. Cabral, N. Nishiyama, K. Kataoka, Optimization of (1,2-diamino-cyclohexane)platinum(II)-loaded polymeric micelles directed to improved tumor targeting and enhanced antitumor activity. *J. Control. Release* **121**, 146–155 (2007).
25. N. D. Sonawane, J. R. Thiagarajah, A. S. Verkman, Chloride concentration in endosomes measured using a ratioable fluorescent Cl^- indicator: Evidence for chloride accumulation during acidification. *J. Biol. Chem.* **277**, 5506–5513 (2002).
26. N. Nishiyama, F. Koizumi, S. Okazaki, Y. Matsumura, K. Nishio, K. Kataoka, Differential gene expression profile between PC-14 cells treated with free cisplatin and cisplatin-incorporated polymeric micelles. *Bioconjug. Chem.* **14**, 449–457 (2003).
27. I. D. Johnson, H. C. Kang, R. P. Haugland, Fluorescent membrane probes incorporating dipyrrometheneboron difluoride fluorophores. *Anal. Biochem.* **198**, 228–237 (1991).
28. S. Arnould, I. Hennebelle, P. Canal, R. Bugat, S. Guichard, Cellular determinants of oxaliplatin sensitivity in colon cancer cell lines. *Eur. J. Cancer* **39**, 112–119 (2003).
29. L. Kelland, The resurgence of platinum-based cancer chemotherapy. *Nat. Rev. Cancer* **7**, 573–584 (2007).
30. E. Raymond, S. Faivre, S. Chaney, J. Woynarowski, E. Cvitkovic, Cellular and molecular pharmacology of oxaliplatin. *Mol. Cancer Ther.* **1**, 227–235 (2002).
31. F. R. Luo, T. Y. Yen, S. D. Wyrick, S. G. Chaney, High-performance liquid chromatographic separation of the biotransformation products of oxaliplatin. *J. Chromatogr. B Biomed. Sci. Appl.* **724**, 345–356 (1999).
32. F. R. Luo, S. D. Wyrick, S. G. Chaney, Biotransformations of oxaliplatin in rat blood in vitro. *J. Biochem. Mol. Toxicol.* **13**, 159–169 (1999).
33. R. Duncan, Polymer conjugates as anticancer nanomedicines. *Nat. Rev. Cancer* **6**, 688–701 (2006).
34. T. Yamori, A. Matsunaga, S. Sato, K. Yamazaki, A. Komi, K. Ishizu, I. Mita, H. Edatsugi, Y. Matsuba, K. Takezawa, O. Nakanishi, H. Kohno, Y. Nakajima, H. Komatsu, T. Andoh, T. Tsuruo, Potent antitumor activity of MS-247, a novel DNA minor groove binder, evaluated by an *in vitro* and *in vivo* human cancer cell line panel. *Cancer Res.* **59**, 4042–4049 (1999).
35. S. Yaguchi, Y. Fukui, I. Koshimizu, H. Yoshimi, T. Matsuno, H. Gouda, S. Hirono, K. Yamazaki, T. Yamori, Antitumor activity of ZSTK474, a new phosphatidylinositol 3-kinase inhibitor. *J. Natl. Cancer Inst.* **98**, 545–556 (2006).
36. A. Vekris, D. Meynard, M. C. Haaz, M. Bayssas, J. Bonnet, J. Robert, Molecular determinants of the cytotoxicity of platinum compounds: The contribution of *in silico* research. *Cancer Res.* **64**, 356–362 (2004).
37. S. L. Kelley, A. Basu, B. A. Teicher, M. P. Hacker, D. H. Hamer, J. S. Lazo, Overexpression of metallothionein confers resistance to anticancer drugs. *Science* **241**, 1813–1815 (1988).
38. J. Holford, P. J. Beale, F. E. Boxall, S. Y. Sharp, L. R. Kelland, Mechanisms of drug resistance to the platinum complex ZD0473 in ovarian cancer cell lines. *Eur. J. Cancer* **36**, 1984–1990 (2000).
39. P. M. Deegan, I. S. Pratt, M. P. Ryan, The nephrotoxicity, cytotoxicity and renal handling of a cisplatin-methionine complex in male Wistar rats. *Toxicology* **89**, 1–14 (1994).
40. R. M. Goldberg, D. J. Sargent, R. F. Morton, C. S. Fuchs, R. K. Ramanathan, S. K. Williamson, B. P. Findlay, H. C. Pitot, S. R. Alberts, A randomized controlled trial of fluorouracil plus leucovorin, irinotecan, and oxaliplatin combinations in patients with previously untreated metastatic colorectal cancer. *J. Clin. Oncol.* **22**, 23–30 (2004).
41. D. Wang, S. J. Lippard, Cellular processing of platinum anticancer drugs. *Nat. Rev. Drug Discov.* **4**, 307–320 (2005).
42. I. Pastan, M. M. Gottesman, K. Ueda, E. Lovelace, A. V. Rutherford, M. C. Willingham, A retrovirus carrying an *MDR1* cDNA confers multidrug resistance and polarized expression of P-glycoprotein in MDCK cells. *Proc. Natl. Acad. Sci. U.S.A.* **85**, 4486–4490 (1988).
43. R. K. Jain, Delivery of molecular and cellular medicine to solid tumors. *Adv. Drug Deliv. Rev.* **46**, 149–168 (2001).
44. Y. Saito, M. Yasunaga, J. Kuroda, Y. Koga, Y. Matsumura, Antitumour activity of NK012, SN-38-incorporating polymeric micelles, in hypovascular orthotopic pancreatic tumour. *Eur. J. Cancer* **46**, 650–658 (2010).
45. M. Mishima, G. Samimi, A. Kondo, X. Lin, S. B. Howell, The cellular pharmacology of oxaliplatin resistance. *Eur. J. Cancer* **38**, 1405–1412 (2002).

46. Y. Akiyama, Y. Nagasaki, K. Kataoka, Synthesis of heterotelechelic poly(ethylene glycol) derivatives having α-benzaldehyde and ω-pyridyl disulfide groups by ring opening polymerization of ethylene oxide using 4-(diethoxymethyl)benzyl alkoxide as a novel initiator. *Bioconjug. Chem.* **15**, 424–427 (2004).
47. N. Nishiyama, S. Okazaki, H. Cabral, M. Miyamoto, Y. Kato, Y. Sugiyama, K. Nishio, Y. Matsumura, K. Kataoka, Novel cisplatin-incorporated polymeric micelles can eradicate solid tumors in mice. *Cancer Res.* **63**, 8977–8983 (2003).
48. W. H. Daly, D. Poche, The preparation of N-carboxyanhydrides of α-amino acids using bis(trichloromethyl)carbonate. *Tetrahedron Lett.* **29**, 5859–5862 (1988).
49. Y. Matsumoto, T. Nomoto, H. Cabral, Y. Matsumoto, S. Watanabe, R. J. Christie, K. Miyata, M. Oba, T. Ogura, Y. Yamasaki, N. Nishiyama, T. Yamasoba, K. Kataoka, Direct and instantaneous observation of intravenously injected substances using intravital confocal micro-videography. *Biomed. Opt. Express* **1**, 1209–1216 (2010).
50. **Acknowledgments:** M.M. thanks J. Ghaugas for his support and suggestions for preparing the manuscript and S. Hiro for his help with in silico data analysis. **Funding:** This research was supported in part by Funding Program for World-Leading Innovative R&D on Science and Technology (FIRST Program) from the Japan Society for the Promotion of Science (JSPS) and the Core Research Program for Evolutional Science and Technology (CREST) from the Japan Science and Technology Agency (JST). **Author contributions:** M.M. and H.C. designed and performed the experiments, analyzed the results, and wrote the manuscript. Y.M. performed the imaging experiments. S.W. performed the siRNA knockdown studies. T.Y. conducted human cell panel analysis. M.R.K. edited the manuscript. N.N. supervised the project and wrote the manuscript. K.K. supervised the project and edited the manuscript. **Competing interests:** The authors declare that they have no competing interests.

Submitted 14 June 2010
Accepted 10 December 2010
Published 5 January 2011
10.1126/scitranslmed.3001385

Citation: M. Murakami, H. Cabral, Y. Matsumoto, S. Wu, M. R. Kano, T. Yamori, N. Nishiyama, K. Kataoka, Improving drug potency and efficacy by nanocarrier-mediated subcellular targeting. *Sci. Transl. Med.* **3**, 64ra2 (2011).

Published OnlineFirst August 4, 2010; DOI: 10.1158/0008-5472.CAN-10-0303

Cancer Research

Visible Drug Delivery by Supramolecular Nanocarriers Directing to Single-Platformed Diagnosis and Therapy of Pancreatic Tumor Model

Sachiko Kaida, Horacio Cabral, Michiaki Kumagai, et al.

Cancer Res 2010;70:7031-7041. Published OnlineFirst August 4, 2010.

Published OnlineFirst August 4, 2010; DOI: 10.1158/0008-5472.CAN-10-0303

Integrated Systems and Technologies

Cancer Research

Visible Drug Delivery by Supramolecular Nanocarriers Directing to Single-Platformed Diagnosis and Therapy of Pancreatic Tumor Model

Sachiko Kaida[1,3,7], Horacio Cabral[1,3], Michiaki Kumagai[1], Akihiro Kishimura[2], Yasuko Terada[4], Masaki Sekino[5], Ichio Aoki[6], Nobuhiro Nishiyama[1,3], Toru Tani[7], and Kazunori Kataoka[1,2,3]

Abstract

Nanoparticle therapeutics are promising platforms for cancer therapy. However, it remains a formidable challenge to assess their distribution and clinical efficacy for therapeutic applications. Here, by using multifunctional polymeric micellar nanocarriers incorporating clinically approved gadolinium (Gd)–based magnetic resonance imaging contrast agents and platinum (Pt) anticancer drugs through reversible metal chelation of Pt, simultaneous imaging and therapy of an orthotopic animal model of intractable human pancreatic tumor was successfully performed without any serious toxicity. The strong tumor contrast enhancement achieved by the micelles correlated with the 24 times increase of r_1 of the Gd chelates, the highest for the formulations using clinically approved Gd chelates reported to date. From the microsynchrotron radiation X-ray fluorescence spectrometry scanning of the lesions, we confirmed that both the Gd chelates and Pt drugs delivered by the micelles selectively colocalized in the tumor interior. Our study provides new insights for the design of theranostic micelles with high contrast enhancement and site-specific clinical potential. *Cancer Res; 70(18); 7031–41. ©2010 AACR.*

Introduction

Recently, there has been explosive development of chemotherapeutic agents for cancer, but the efficacies of anticancer drugs are still insufficient particularly for the treatment of intractable tumors, including pancreatic cancer. Although the latest advances in molecular targeting agents have shown specific efficiency, the survival time of patients is often extended only slightly, even when these agents are used in combination with other anticancer drugs. Moreover, the use of such drugs typically results in various characteristic side effects, such as interstitial pneumonia for gefitinib (1), cardiotoxicity for trastuzumab (2, 3), and thrombosis for bevacizumab (4). Alternatives to developing these compounds and antibodies selective for cancer cells, with the aim of modulating drug distribution in the body to accomplish selective drug accumulation in the tumor site, are thus needed, and for this purpose, nanometric-scale vehicles or nanocarriers directing therapeutics to the tumor site are a key platform.

In the last decade, several kinds of nanoparticle therapeutics platforms, including liposomes, nanoparticles, and polymeric micelles, have been developed to selectively deliver drugs to tumor sites (5–12). These approaches have been used to improve the therapeutic efficacy and to reduce the side effects of drugs incorporated in delivery carriers (13, 14), and nanoparticle therapeutics such as Doxil (15) or Abraxane (16) are already in clinical use. The tumor targeting of these nanoparticle therapeutics is based on the enhanced permeability and retention (EPR) effect (in other words, the increased accumulation of high–molecular weight compounds, such as nanoparticles, in tumor tissue due to the high permeability of tumor blood vessels and the retention of these compounds because of the impaired lymphatic drainage at the cancer site; ref. 17). In the late 1980s, we developed one of the auspicious nanoparticle therapeutics, polymeric micelles, a self-assembly of amphiphilic block copolymers consisting of hydrophobic segments forming the drug-loaded core and water-soluble segments forming the biocompatible shell (11, 12). The main advantages of this system are the possibility of incorporating a variety of drugs, including hydrophobic substances, metal complexes, and charged macromolecules such as nucleic acids, as well as controlling their release properties by engineering and modifying the micelle-forming block copolymers. Moreover, polymeric micelles can be designed to be responsive to environmental changes and capable of target

Authors' Affiliations: [1]Center for Disease Biology and Integrative Medicine, Graduate School of Medicine, [2]Department of Materials Engineering, Graduate School of Engineering, and [3]Center for NanoBio Integration, The University of Tokyo, Tokyo, Japan; [4]Japan Synchrotron Radiation Research Institute, SPring-8, Hyogo, Japan; [5]Department of Advanced Energy, Graduate School of Frontier Sciences, The University of Tokyo, Chiba, Japan; [6]Molecular Imaging Center, National Institute of Radiological Sciences, Chiba, Japan; and [7]Department of Surgery, Shiga University of Medical Science, Shiga, Japan

Note: Supplementary data for this article are available at Cancer Research Online (http://cancerres.aacrjournals.org/).

Corresponding Author: Kazunori Kataoka, Department of Materials Engineering, Graduate School of Engineering, The University of Tokyo, 7-3-1 Hongo, Bunkyo-ku, Tokyo 113-8656, Japan. Phone: 81-3-5841-7138; Fax: 81-3-5841-7139; E-mail: kataoka@bmw.t.u-tokyo.ac.jp.

doi: 10.1158/0008-5472.CAN-10-0303

Published OnlineFirst August 4, 2010; DOI: 10.1158/0008-5472.CAN-10-0303

recognition. Our micelle formulations incorporating Adriamycin, paclitaxel, SN-38, cisplatin, and DACHPt (activated oxaliplatin; NK911, NK105, NK012, NC6004, and NC4016, respectively) are being examined in clinical studies, and four of these formulations have advanced to phase II studies (18–21). These clinical studies have revealed that polymeric micelles showed reduced side effects and high effectiveness against various intractable tumors, including triple-negative breast cancers that do not express the genes for estrogen receptor, progesterone receptor, and Her2/neu (22). Consequently, polymeric micelles have been considered one of the most promising drug delivery systems (DDS) in the field of cancer chemotherapy.

Although a crucial breakthrough in cancer treatment has been achieved using several micelles, the methods for estimating the distribution and effectiveness of the micelles are ineffective and inadequate. The precise monitoring of their distribution and early feedback on treatment efficacy would allow clinicians to anticipate the therapeutic process in each cancer patient and customize medicine for cancer therapy. Thus, it is imperative to directly assess the biodistribution of the micelles and their cargo as well as the magnitude of their accumulation at the cancer site. Consequently, the development of micelles with both imaging and therapeutic functions [theranostic (23) micelles] will permit visualization of the distribution of the micelles inside the body and tumor in a real-time manner, allowing optimization of the treatment protocol according to the unique characteristics of the malignancies in individual patients (24–26).

We developed theranostic core-shell polymeric micelles based on the self-assembly of block copolymers with both a magnetic resonance imaging (MRI) function and cancer therapeutic capacity. The micelles incorporate gadolinium–diethylenetriaminepentaacetic acid (Gd-DTPA), a widely used T_1-weighted MRI (T1W) contrast agent (27), and (1,2-diaminocyclohexane)platinum(II) (DACHPt), the parent complex of the potent anticancer drug oxaliplatin, in their core by reversible complexation between DACHPt, Gd-DTPA, and poly(ethylene glycol)-*b*-poly(glutamic acid) [PEG-*b*-P(Glu); Fig. 1]. Accordingly, both the DACHPt and Gd-DTPA complexes, which can be excreted from the kidney, thus avoiding toxicity from long-term accumulation inside the body, are released from the micelles in a sustained manner under physiologic conditions. Moreover, the longitudinal relaxivity (r_1) of the micelles (i.e., their ability as an MRI contrast agent) increased ~24 times compared with that of free

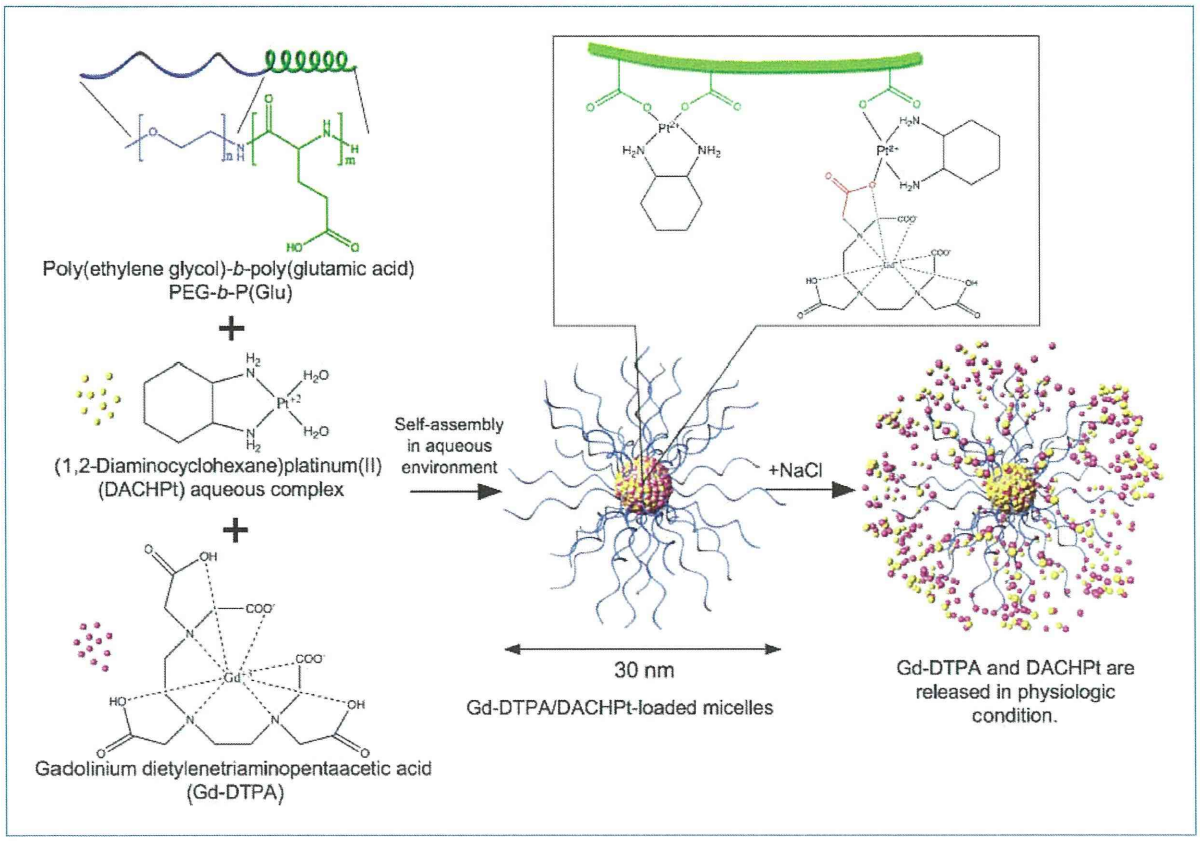

Figure 1. Schematic diagram of proposed self-assembly of Gd-DTPA/DACHPt–loaded micelles and release of Pt and Gd complexes from the micelles in chloride-containing medium.